Chapter 2

Second Harmonic Generation in ZnO Nanowires

Soumen Dhara and Stephen A. Lynch

Additional information is available at the end of the chapter

http://dx.doi.org/10.5772/intechopen.68150

Abstract

Second harmonic generation (SHG) is one of the most researched nonlinear material properties and finds applications in many fields ranging from laser projection to cancer detection to future optical switches for molecular devices. Studying SHG in ZnO nanostructures started few years ago and there is a long way to go to compete with the existing nonlinear crystals. Information gathered over the past few years in research on SHG of ZnO nanowires (NWs) is summarized in this chapter. Recent advancement in the growth techniques for various types of ZnO NWs used for SHG studies is also discussed. We present an extensive analysis and discussion on some key parameters that directly modify the efficiency of SHG in ZnO NWs. The key parameters considered for discussion are aspect ratio of NWs, doping, and external strain. At the end, current standing on the reported values of nonlinear coefficients and future outlook are presented.

Keywords: second harmonic generation, sum frequency generation, ZnO, symmetry deviation

1. Introduction

ZnO is a unique material with application prospects in areas ranging from medical to optoelectronic industry to astronomical radiation detection [1–5]. ZnO is a II–VI group wide-band gap semiconductor and is highly transparent in the visible region. In the hexagonal wurtzite phase of ZnO, each Zn ion is surrounded by a tetrahedron of four O ions and vice versa. This tetrahedral coordination results in a noncentrosymmetric crystal structure, which makes it a promising candidate to observe second harmonic generation (SHG) in ambient conditions. SHG is a second-order nonlinear coherent process in which two lower energy photons are up-converted to a single photon with frequency exactly twice the incident frequency. This interesting property of nonlinear materials has several important applications in various fields, e.g., probing the electronic and magnetic structure of crystals, cancer cell diagnostics, switches in molecular-scale memory devices, and many more [6–10]. It is a very sensitive all-optical and noninvasive technique that is compatible with bulk or surface detection under various circumstances.

Among the huge variety of ZnO nanostructures, nanorods and nanowires (NWs) have undoubtedly been the focus of most studies since their geometries allow the preparation of arrays of well-controlled uniformity and use as building blocks of many nanoscale devices. As well as for ZnO thinfilms, SHG from ZnO NWs grown by different methods has been widely investigated. Studying SHG in ZnO NWs started few years ago and lot of information/knowledge has been gathered over the years by the nanoscale research community. Previous studies reported efficient generation of SHG signal from various types of ZnO nanostructures, including NWs [11–20]. Therefore, with improvement in the fabrication technique for large area ZnO NWs, it can be widely used as one of the best SHG materials. It has been discovered that the magnitude of SHG is strongly influenced by crystal orientation, aspect ratio, crystal symmetry modification, and so on. Therefore, by controlling such parameters one can tune the SHG of ZnO NWs. However, effective implementation of the knowledge gathered over the past years to ZnO to get the best SHG performance is yet to be achieved. Strategies for raising the optical nonlinearities of materials are an active research theme with rich and broad implications/applications. Keeping this in mind, some previous studies attempted to improve the second-order nonlinearity of ZnO and developed some efficient methodologies. Very high values of susceptibility tensorial component of 22–30 pm/V were achieved by changing the crystallographic orientation or decorating the surface with metal nanoparticles followed by bicolor coherent treatment or doping-induced crystal symmetry deviation [20–23]. Recently, development of ZnO-based SHG microscopy has been successfully demonstrated [24, 25].

Presently there is no review article dedicated to SHG of ZnO NWs with extensive analysis of SHG parameters and up-to-date advancement in this field. In this chapter, we present an extensive review of recent advances in SHG from ZnO NWs including our own results. Following this brief introduction, crystal structure of ZnO and theoretical background of SHG from ZnO and nonvanishing second-order nonlinear tensorial components are presented in Section 2. Section 3 describes the methodology adopted to measure SHG and an extensive analysis of the associated susceptibility tensor components. Recent advancement in the growth techniques for various types of ZnO NWs used for SHG studies and their SHG characteristics is discussed in the next section. The effects of aspect ratio of NWs, doping, and external strain on SHG magnitude are extensively addressed in subsections. At the end, a summary of the current standing on the reported values of nonlinear coefficients and future outlook are presented.

2. Second harmonic generation

SHG is one of the most studied material properties since its discovery in the 1960s by Franken et al. [26]. It is also known as the sum frequency generation because of the frequency doubling effect. When a strong primary radiation beam (frequency ω) is fed into the NLO crystal, along with the transmitted primary beam an additional light beam (frequency 2ω) appears from the crystal with frequency twice that of the primary beam. In other words, wavelength of the SHG signal is exactly half of the wavelength of the incident primary beam. **Figure 1** depicts the schematic illustration of nonlinear optical process SHG. Most often, the polarization field is considered to be linearly related to the incident electric field

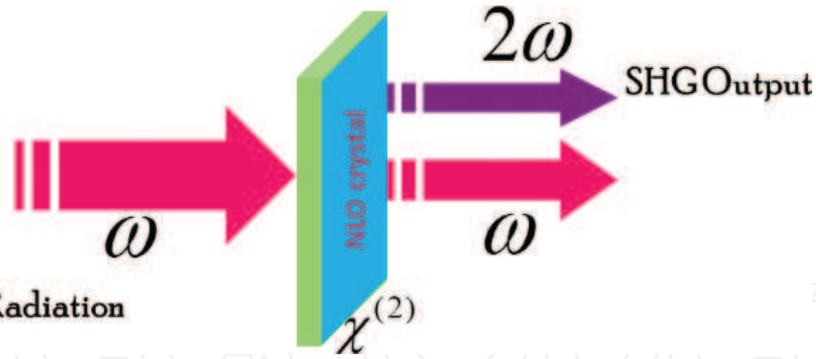

Figure 1. Schematic diagram of SHG in NLO crystal.

$$\vec{P} = \epsilon_0 \chi \vec{E} \tag{1}$$

where the electrical susceptibility, χ is a second-rank tensor. While this consideration tends to be sufficient when relating incident fields at low field strengths, it is a simplified approximation. In reality, the polarization field is more complicated than the linear relation given above. If the variation is small under strong electric field, comparable to interatomic electric fields, the polarization can be exactly expressed with the help of Taylor series

$$P_i = \epsilon_0(\chi_{ij}^{(1)}\ E_j + \chi_{ijk}^{(2)}\ E_j E_k + \chi_{ijkl}^{(3)}\ E_j E_k E_l + \ldots) \tag{2}$$

where terms are summed over repeated indices. The first coefficient $\chi_{ij}^{(1)}$ is the linear electric susceptibility component. The $\chi_{ijk}^{(2)}$ and $\chi_{ijkl}^{(3)}$ are second-order and third-order nonlinear susceptibilities responsible for SHG and third harmonic generation phenomenon. The second-order susceptibility tensor is also expressed in terms of nonlinear optical coefficients, $d_{ijk} = \frac{1}{2}\chi_{ijk}^{(2)}$. SHG arises only when the particular material has nonzero second-order susceptibility tensor, $\chi_{ijk}^{(2)}(-2\omega,\ \omega,\ \omega)$. The nonzero components exist only in the noncentrosymmetric crystal structure of the particular material. Furthermore, nanometer-sized centrosymmetric materials (nanostructures) also show weak SHG due to the breaking of space inversion symmetry at the boundary [27, 28].

The crystal structures shared by ZnO are wurtzite, zinc blende, and rocksalt; however, in ambient condition, only the wurtzite phase is thermodynamically stable. The wurtzite structure has a hexagonal unit cell with two lattice parameters, *a* and *c*, in a ratio of *c*/*a* = 1.633 and belongs to the space group of C6*v*4 or *P*63*mc*. The hexagonal lattice of ZnO is characterized by two interconnecting sub-lattices of Zn^{2+} and O^{2-}, such that each Zn ion is surrounded by a tetrahedron of O ions, and vice versa, which is shown in **Figure 2**. The tetrahedral coordination in ZnO results in noncentral symmetric structure. Another important characteristic of ZnO is the polar surfaces. The most common polar surface is the basal plane. The oppositely charged ions produce positively charged Zn-(0001) and negatively charged O-$(000\overline{1})$ polar surfaces, resulting in a normal dipole moment and spontaneous polarization along the *c*-axis. The (001) polar face along the *c*-axis is the primary growth orientation of ZnO.

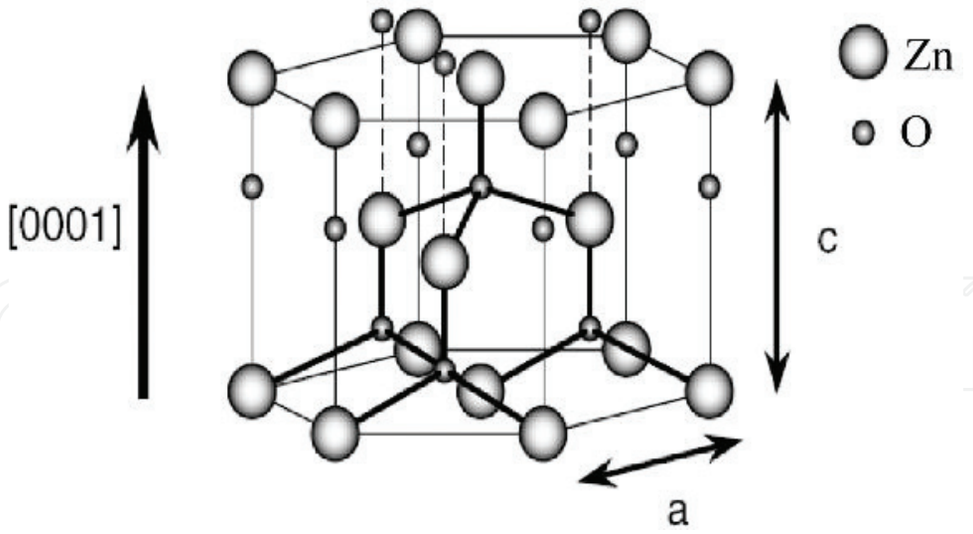

Figure 2. The wurtzite crystal structure model of ZnO having lattice constants *a* in the basal plane and *c* in the basal direction.

As a consequence of noncentrosymmetric crystal structure, ZnO possess nonvanishing second-order susceptibility tensor. The *c*-axis-grown vertically aligned ZnO NWs present five nonvanishing second-order susceptibility tensor elements, which are governed by point group symmetry of wurtzite crystal structure. The values of these second-order tensors or nonlinear optical coefficients are represented in pm/V. Five nonvanishing susceptibility tensorial components are $\chi_{15}^{(2)}$, $\chi_{24}^{(2)}$, $\chi_{31}^{(2)}$, $\chi_{32}^{(2)}$ and $\chi_{33}^{(2)}$ or equivalent in nonlinear optical coefficients d_{15}, d_{24}, d_{31}, d_{32}, and d_{33}. The point group symmetry *P*63*mc* of ZnO further reduces the nonvanishing terms to three components, d_{15} ($d_{15} = d_{24}$), d_{31} ($d_{31} = d_{32}$), and d_{33}. In ideal wurtzite structure, Kleinman's symmetry rule can be applied in a condition where the SHG wavelength is far from the absorption resonance. Within this approximation, $d_{15} = d_{31}$ is allowed and the number of independent d_{ij} terms further reduces to two.

3. Measurement technique and methodology

Since its introduction, several experimental techniques have been developed to calculate the magnitude of nonvanishing macroscopic nonlinear coefficients. Out of several techniques, the Maker fringes technique [29] is widely used to determine the magnitude of second-order susceptibility tensor elements. In brief, an SHG signal transmitted through the nonlinear crystal was measured as a function of angle of incidence of the fundamental beam with respect to the sample plane. This method is based on analysis of variation of SHG magnitude by incidence angle of the fundamental beam and crystal thickness. A schematic block diagram of the standard Maker fringes-based SHG measurement setup is shown in **Figure 3**. To generate SHG signal, we used an 800 nm, mode-locked femtosecond pulse light source from Ti:sapphire laser as a primary radiation. The polarization state of the fundamental beam and SHG signal are selected by using a polarizer ($\lambda/2$ plate) before the sample and an analyzer after the sample. The laser beam is tightly focused on the sample using suitable mirrors and lens assembly. The

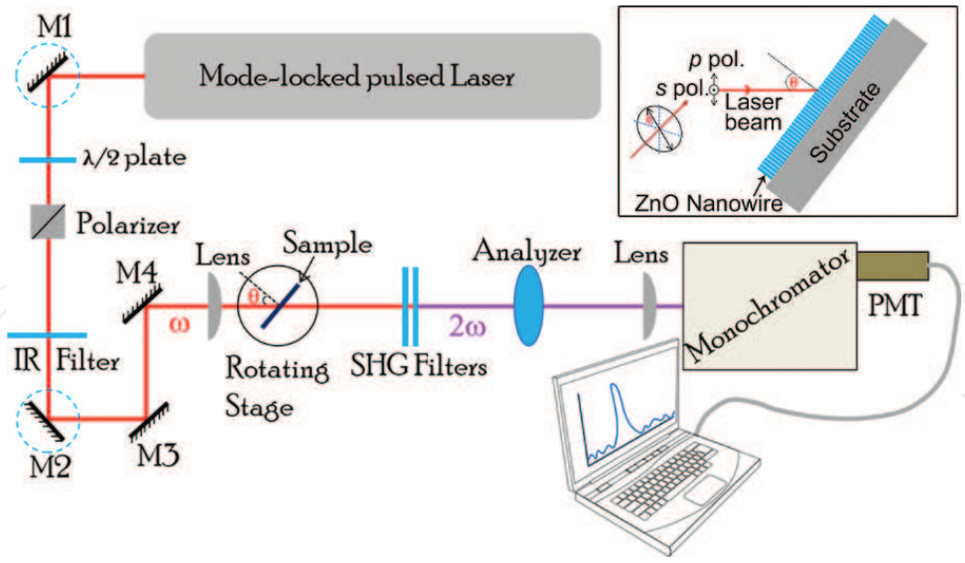

Figure 3. Schematic block diagram of SHG measurement setup according to the Maker fringes technique. Inset shows the ZnO nanowire film with the incident laser beam. θ and ϕ represent the incident angle and polarization angle of the laser beam, respectively.

variation of angle of incidence (θ) is achieved by placing the sample on a rotating stage. The generated SHG signal is analyzed using a monochromator and a highly sensitive detector. The angular dependence of SHG signal is measured either in P-in/P-out (*p*-*p*) or in S-in/P-out (*s*-*p*) polarization configuration.

The original Maker fringes methodology was based on the assumption of 100% transparency of the material in the SHG wavelength region. It is perfectly applicable only to a 100% transparent crystal. However, none of the real crystals are perfectly transparent up to that level. The original Maker fringes methodology failed to correctly estimate magnitude of the second-order d_{ij} values and large errors occur for absorbing materials. To take into account the absorption effect of the crystal in fundamental (ω) and SHG (2ω) wavelength regions, Herman and Hayden [30] presented a modified version of Maker fringes equation. According to Herman et al., the intensity of the second harmonic signal of Maker fringes, when the sample has significant absorption in the SHG wavelength region, is given by

$$
\begin{aligned}
&P_{2\omega}^{x-p}(\theta,\lambda) = \frac{128\pi^3}{cA}\frac{[t_{af}^{\omega}]^4[t_{fs}^{2\omega}]^2[t_{sa}^{2\omega}]^2}{n_2^2c_2^2}\left(\frac{2\pi L}{\lambda}\right)^2 d_{eff}^2\, P_{\omega}^2 \times \exp[-2(\delta_1+\delta_2)]\frac{\sin^2\psi+\sinh^2\chi}{\psi^2+\chi^2}\\
&\psi = \left(\frac{2\pi L}{\lambda}\right)(n_1c_1 - n_2c_2)\\
&\delta_1 = \left(\frac{2\pi L}{\lambda}\right)\left(\frac{n_1\kappa_1}{c_1}\right), \delta_2 = \left(\frac{2\pi L}{\lambda}\right)\left(\frac{n_2\kappa_2}{c_2}\right), \chi = \delta_1 - \delta_2\\
&[t_{af}^{\omega}] = \begin{cases} \dfrac{2cos\theta}{c_1 + n_1cos\theta}, & x = p \\ \dfrac{2cos\theta}{n_1c_1 + cos\theta}, & x = s \end{cases}, [t_{fs}^{2\omega}] = \frac{2n_2c_2}{n_{2s}c_2 + n_2c_{2s}}, [t_{sa}^{2\omega}] = \frac{2n_{2s}c_{2s}}{n_{2s}cos\theta + c_{2s}}
\end{aligned}
\tag{3}
$$

where $[t_{ij}^{k}]$ are the Fresnel transmission coefficients of fundamental (ω) and SHG (2ω) wavelength regions at different interfaces; *af*—air to film, *fs*—film to substrate and *sa*—

substrate to air. c and A are velocity of light and the area of the laser beam spot; P_ω and $P_{2\omega}$ are the power of the incident beam and the SHG output; L is the thickness of the film. Remaining terms in Eq. (3) arise from the absorption of ZnO and phase mismatch parameter (Ψ). The complex refractive index is $n_m = n_m(1+ ik_m)$ and $c_m = (1–(1/n_m)^2 \sin^2\theta)^{1/2}$. Subscripts 1, 2 are the fundamental beam and second harmonics, respectively. Finally, the term d_{eff} represents effective optical nonlinear coefficient, arising from the second-order nonlinear optical tensor. The general expression for d_{eff} is a bit complicated, being dependent on the polarization states of both first and second harmonic electric fields, respectively, and, of course, on the angle of incidence of the fundamental beam. Considering the ZnO group symmetry and Kleinman's symmetry approximation, the final expressions for d_{eff} for p and s polarization configurations are,

$$d_{eff} = \begin{cases} 2d_{31}c_1c_2 sin\theta/n_1 + d_{31}c_1^2 sin\theta/n_2 \; + \; d_{33} sin^3\theta/n_1^2 n_2, & x = p \\ \dfrac{d_{31} sin\theta}{n_2}, & x = s \end{cases} \tag{4}$$

Therefore, at a monochromated fundamental beam of fixed wavelength (λ), the intensity of the SHG in Eq. (3) can be simplified as a function of θ only. After fitting Eq. (3) into the measured SHG profile as a function of angle of incidence, one can estimate the associated d_{eff} value. In *s-p* configuration, d_{eff} depends only on d_{31}. By fitting the SHG signal data, one can obtain the value of the coefficient d_{31} which can be introduced into data fitting in the *p-p* configuration to calculate d_{33}. In another way, the d_{eff} value can be more accurately estimated by considering Eq. (3) as a function of wavelength (λ) only [14, 20]. This method minimizes error due to the Gaussian profile broadening of the fundamental beam with finite full width at half maximum (FWHM). At a fixed incident angle (θ), Eq. (3) can be adapted in the given form

$$\mathrm{P}_{2\omega}^{p-p}(\lambda) = [\mathrm{P}_{2\omega(\lambda)}^{p-p}]' \mathrm{P}_{\omega(\lambda)}^2 \left(\frac{2\pi \mathrm{L}}{\lambda}\right)^2 \mathrm{d}_{\text{eff}}^2 \tag{5}$$

where $P_{\omega(\lambda)}$ is the relative power of the primary beam at a particular wavelength, λ.

Alternative to Maker fringes experimental configuration, the reflective second harmonic generation (RSHG) scheme involves the measurement of the SHG signal in reflection mode, at a fixed incidence angle and as a function of the azimuthal angle, which is the angle between the incidence plane and the x-axis on the sample surface. In brief, the sample is rotated along its surface normal, *i.e.*, along the z-axis, while the reflected SHG signal is systematically measured. The RSHG signals originating from the symmetry of ZnO crystal as a function of the azimuthal angle ϕ are given by

$$\mathrm{P}_{2\omega}^{x-p} = \begin{cases} d_{15}\mathrm{E}_0^2\hat{x} + \dfrac{1}{2}(\, d_{31} + d_{33})\mathrm{E}_0^2\hat{z}, & x = p \\ d_{31}\mathrm{E}_0^2\hat{z}, & x = s \end{cases} \tag{6}$$

The RSHG is independent of azimuthal angle, if the direction of ZnO (0002) is along the z-axis. However, a tilt of the ZnO (0002) direction may cause a variation of the resulting SHG on the azimuthal polar plot.

4. Second harmonic generation in ZnO nanowires

As a consequence of noncentrosymmetric structure, ZnO is expected to possess nonzero second-order optical nonlinearity parameters and hence room temperature SHG is expected. SHG from ZnO nanostructures including NWs has been experimentally demonstrated by several groups. Many efforts have been made to quantitatively estimate the second-order nonlinear coefficients of single ZnO NWs or ZnO NW arrays. A theoretical study on the estimation of SHG intensity from ZnO nanostructures was done by Attaccalite et al. [31]. The modified Maker fringes equation was employed by considering the dense NW arrays as a NW film. All the important experimental results on SHG of ZnO NWs are summarized in **Table 1**.

Chan et al. [13] show room temperature SHG from ZnO NWs with angular dependence exactly similar to thinfilms. Vertically aligned ZnO NWs were grown on the ZnO-seeded glass substrate by low temperature aqueous chemical solution method, which is shown in **Figure 4 (a)**. Following the reaction at 90°C, glass substrates were rinsed with de-ionized water to remove the residual salt on the surface, and then dried at 100°C. The average length of the ZnO NWs ranged from 50 to 700 nm. A Q-switched Nd:YAG laser was used as fundamental incident beam (λ = 1064 nm, 8 ns) at 10 Hz frequency. SHG signal from samples was detected by a photo-multiplier tube and then further processed with a signal-integrating oscilloscope. The variation of SHG intensity with the angle of incidence depicts periodic profile and obeys the Maker fringes methodology (**Figure 4(b)**). The second-order coefficients d_{31} and d_{33} were estimated after fitting to the experimental angular variation of SHG data by Maker fringes Eq. (3) and were found to be d_{31} = 1.28 and d_{33} = −15.7 pm/V.

The nonlinear second-order coefficients, d_{ij} can also be estimated precisely in another way by fitting the experimental SHG data with Maker fringes Eq. (5) [14, 20, 32]. The SHG signal was measured at fixed incidence angle, where SHG is maximum as a function of wavelength within the range of Gaussian beam profile. Broadband frequency-doubling properties of *c*-axis-oriented ZnO NW arrays grown by low-temperature chemical bath deposition method on glass substrate were investigated by Das et al. [14]. The measured spectral profile of SHG was found to be in good agreement with theoretical simulations. The generated SHG signals were analyzed using a spectrometer at pumping wavelength of 806 nm (Ti:sapphire laser oscillator at pulse durations ~13 fs and spectral FWHM ~100 nm) and pump intensity of 5.5×10^{10} W/cm^2. The maximum effective nonlinearity was found to be d_{eff} = 15 pm/V, which is about 7.5 times higher than that of a type-I beta-barium borate (BBO) crystal. Changes in the growth parameters in the chemical bath deposition also result in an improvement in the SHG intensity [41].

Our group used similar theoretical fitting method to retrieve the d_{eff} by measuring SHG signal as a function of wavelength. We prepared dense and *c*-axis-oriented ZnO NWs onto quartz substrate by modified aqueous chemical method as shown in **Figure 5(a)** [20]. Highly crystalline ZnO NWs with diameters of 70–100 nm and length of few microns were grown perpendicular to the substrate. The SHG signal was measured by passing a linearly polarized femtosecond pulse beam (at 800 nm) from a mode-locked Ti:sapphire laser through the sample and analyzing in a spectrometer with a spectral resolution of 0.2 nm. At an incident angle (θ) of 0° *i.e.*, when the incident beam is perpendicular to the substrate plane, the magnitude of

Growth technique	Substrate	Laser source	Aspect ratio	d_{ij} (pm/V)	Reference
Sonication and dispersion	Sapphire	fs Laser @800 nm	–	$d_{31} = 1.36$ $d_{33} = -14.3$	Wang et al. [33]
Chemical vapor deposition	Sapphire	fs Laser @800 nm	–	$\chi^{(2)}_{eff} = 5.5$	Johnson et al. [34]
Aqueous solution method	Glass	ns Laser @1064 nm	5.7 10.8	$d_{31} = 0.14$ $d_{33} = 7.8$ $d_{31} = 2.88$ $d_{33} = 18.0$	Chan et al. [13]
Low temperature chemical bath method	Glass	fs Laser @806 nm	23.2 14.7 10.7	$d_{eff} = 15.0$ $d_{eff} = 2.0$ $d_{eff} = 3.2$	Das et al. [14]
Aqueous solution method	–	fs Laser @810 nm	–	$d_{31} = -3.0$ $d_{33} = 0.56$ $d_{33} = 0.86$	Green et al. [35]
Chemical bath deposition	Glass	fs Laser @800 nm	8	$d_{31} = -31.4$ $d_{33} = 2.56$	Das et al. [36]
Hydrothermal method	ITO coated glass	fs Laser @1034 nm	6.0 13.2	$d_{31} = 0.29$ $d_{33} = -1.38$ $d_{31} = 0.99$ $d_{33} = -9.53$	Zhou et al. [37]
Chemical vapor deposition	Si	fs Laser @800 nm	–	$d_{15} = 10.2$	Liu et al. [38]
Modified aqueous chemical method, Europium doping	Quartz	fs Laser @800 nm	–	$d_{eff} = 12.57$ $d_{eff} = 19.09$ after 1% doping	Dhara et al. [20]
Aqueous solution method	Glass	fs Laser @1044 nm	10.0	$d_{33}/d_{31} = 1.11$	Liu et al. [39]
Hydrothermal synthesis, Co doping	Glass	fs Laser @1044 nm	15.5	$d_{31}/d_{31(undoped)} = 1.17$ $d_{33}/d_{33(undoped)} = 2.34$	Liu et al. [40]

Table 1. Summary of SHG results of ZnO NWs.

SHG is almost zero. Then SHG increases with the changes in the tilting axis of the substrate and shows a maximum at an incident angle of –55°, as expected. The polarization dependence of SHG shows a periodic variation (periodicity π for P-in/P-out and $\pi/2$ for S-in/P-out) with changes in the degree of polarization of the incident beam. The incident laser power dependence on the SHG intensity increases with the increase in incident laser power and shows very good linearity with power dependence factor of $\sim 1.91 \pm 0.02$, very close to the reported value (2.02 ± 0.10) for the bulk ZnO crystal [18]. Therefore, the SHG output closely follows the ideal square law dependence on the incident laser power. **Figure 5(b)** shows measured SHG spectral profile of the as prepared ZnO NWs in P-in/P-out polarization configuration at an angle of incidence (θ) of 50°. The estimated second-order nonlinear coefficient (d_{eff}) was found to be 12.57 ± 0.04 pm/V, which is larger than the reported results from ZnO thinfilms [12, 42, 43].

The microscopic SHG mapping of a single ZnO NW was measured for the first time by near-field scanning optical microscopy (NSOM) [34]. For NSOM studies, ZnO NWs were removed

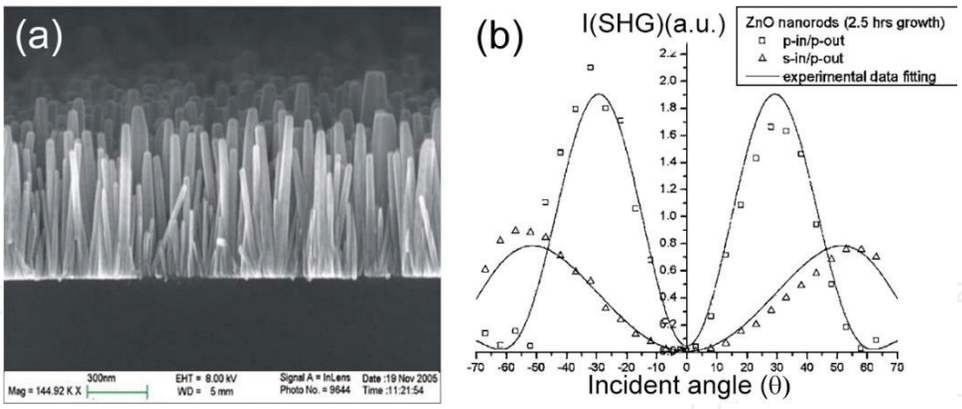

Figure 4. (a) Side-view SEM image of the ZnO nanorods/nanowires grown by aqueous chemical solution method. SHG vs. incident angle (θ) of ZnO nanorods in s-in/p-out and p-in/p-out configurations and their experimental data fittings according to the Maker fringes method. Reproduced with permission from Chan et al. [13] © Springer-Verlag 2006.

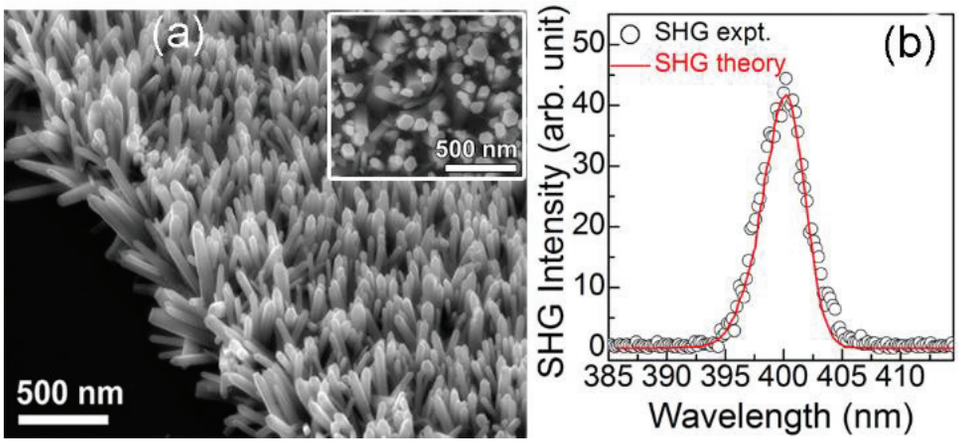

Figure 5. (a) FESEM image (tilted view) of the chemically grown vertically aligned undoped ZnO NWs. Inset shows the top view image of the same ZnO NWs. (b) Spectrum of the measured SHG signal (circle) of the ZnO NWs and theoretical fit (red line). Reproduced with permission from Dhara et al. [20] © IOP Publishing Ltd 2014.

from the substrate by sonication and dispersed onto a flat sapphire substrate for NSOM studies. Near-field SHG wave was collected using a scanning fiber probe at an oblique angle (θ, angle between the surface normal and the fundamental beam k-vector) of 55°. A large nonlinear SHG response with asymmetric variation across the diameter of the NW was presented (**Figure 6**). Furthermore, a strong polarization dependence was evidenced by the SHG images, which is ascribed to the asymmetry of the nonlinear susceptibility. The NW shows relatively efficient SHG with a larger $\chi_{eff}^{(2)}$ = 5.5 pm/V than a BBO crystal, $\chi_{eff}^{(2)} \approx 2.0$ pm/V, a commonly used frequency doubling crystal. However, the estimated highest coefficient ($\chi_{33}^{(2)}$) is considerably lower than the reported bulk value (14.3 pm/V) [33]. One of the possible reasons for lower value is that the number of ZnO molecules probed for a single NW is less than those probed on a solid disk.

Studying SHG sometimes allows us to use a contactless surface as investigation tool to identify structural defects. Similar to thinfilms, if twin defects are present in the NWs, it can be experimentally investigated using SHG mapping to the individual rods [44]. The ZnO rods were grown on fused quartz by the aqueous solution method. The rods (length of several microns and diameter of 100–250 nm) were grown horizontally to the substrate where the polar axes of rods are parallel to the surface of fused quartz, as shown in **Figure 7(a)** and **(b)**. The SHG signal was generated using a mode-locked femtosecond pulse Ti:sapphire laser at approximately 810 nm. The transmitted SHG signals were measured under normal incidence with the polarization direction along the rod's axis. The far-field scattering patterns of the

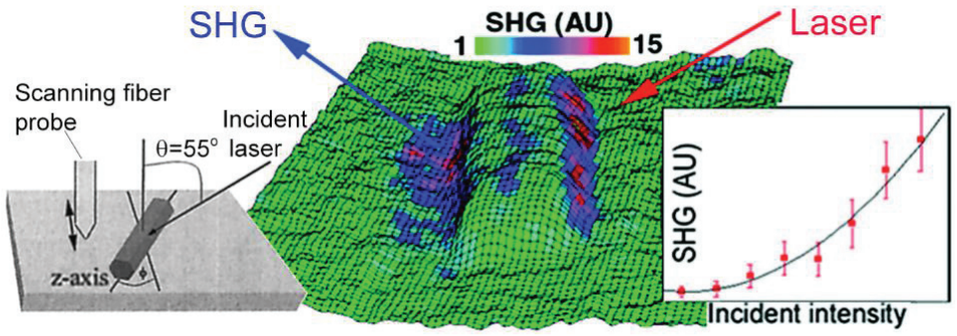

Figure 6. Near-field SHG image of single ZnO NW measured by NSOM. Insets show the illustration of the sample/beam geometry and incident laser power dependence of the SHG signal. Reproduced with permission from Johnson et al. [34] © American Chemical Society 2002.

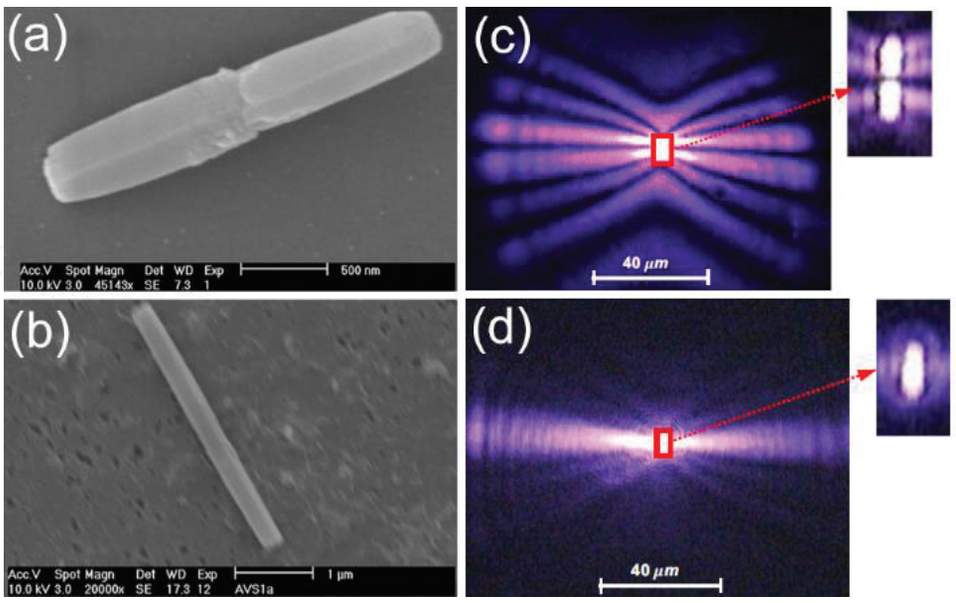

Figure 7. SEM images of two typical ZnO nanowires. (a) ZnO nanowire with twinning boundary structure and (b) ZnO nanowire without the twinning structure. SHG images and scattering patterns for single, (c) twinned ZnO nanowire of length 3.8 μm and (d) twin-free ZnO nanowire of length 1.5 μm. The insets show the enlarged view of above SHG images. Reproduced with permission from Liu et al. [44] ©The American Physical Society 2008.

transmitted SHG waves from single twinned rod were compared to the pattern arising from a twin-free ZnO rod to see if it is possible to differentiate between twinned and twin-free ZnO rods. **Figure 7(c)** and **(d)** shows typical SHG image for a single rod with twinned and twin-free structure, respectively. The images exhibit strong far-field scattering fringes resulting from the interferences of the SHG waves originating from different locations along the axis of the rod. Interestingly, a clear striking difference in the SHG fringes pattern was observed between SHG mapping images of twinned and twin-free rods. In particular, the zero-angle fringes highlight the different features of the two kinds of rods; a bright spot of SHG with a small dark gap for the twinned rod and very wide bright spot with no dark gap for the twin-free rods. A dark (bright) fringe at the 0° scattering angle was ascribed to destructive (constructive) interference of the SHG waves originating from each halve of the twinned (twin-free) rods. A small dark gap with low SHG efficiency (dark fringe) was observed only in the twinned rod, which indicates the existence of twin defects. Furthermore, use of polarization-dependent SHG microscopy to efficiently detect the lattice distortion in single-bent ZnO NWs has been demonstrated [25].

From SHG studies, it is found that SHG signal from bulk ZnO or even ZnO nanostructures is not so strong for application purpose. The reported value of an effective second-order tensorial component varies from 2 to 15 pm/V. However, it could be improved further by proper control of its crystal structure and disturbing crystal symmetry. Many studies have shown dependence of nonlinear parameters on various factors (internal or external to ZnO NWs) and also demonstrated several methods to improve the SHG further. Effects of some of the important parameters on the SHG are discussed in the following subsections. Recent advancement suggests that it is possible, in principle, for the researchers to identify the crystalline orientation, symmetry deviation, and polarities in more complicated ZnO nanostructures by the SHG patterns.

4.1. Wavelength dependence

When SHG was measured near the resonance region of ZnO, in most of the studies SHG signal was detected along with two-photon photoluminescence (2PL). Considering the different nonlinear mechanisms of both the process, final output intensities strongly depend on both pumping wavelength and light intensity. Competition between SHG and 2PL was observed and explained in several works [45–48]. Measuring emitted light as a function of fundamental beam wavelength is a useful way to distinguish the different contributions of SHG and 2PL to the emission spectrum. SHG wavelength changes according to the change in fundamental beam wavelength, while the wavelength of 2PL is fixed by the ZnO band gap energy. The competition between SHG and 2PL as a function of pump wavelength was described by Pedersen et al. [45] in randomly oriented ZnO NWs (**Figure 8(a)**). The monochromator was scanned over a broad region around SHG wavelength for a wide spectral range from 710 to 1000 nm. The contour plot that depicts the structure with highest intensity is the SHG signal at half the pump wavelength, while the weaker horizontal structure is multi-photon excited luminescence from the ZnO band gap. When the 2PL appears at shorter wavelengths than SHG (below the SHG line), it is presumably multiple-photon luminescence while the much stronger two-photon process is seen above the SHG line. The normalized $d_{\text{eff,}}$ retrieved from

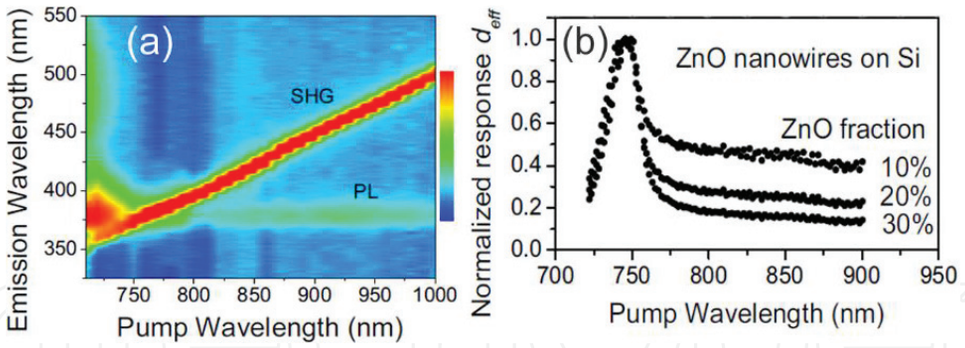

Figure 8. (a) Contour plot showing light emission intensity as a function of pump emission wavelength from ZnO nanowires. Structures due to SHG and multi-photon photoluminescence are marked. (b) Normalized effective nonlinear response of ZnO nanowires as a function of the pump wavelength. Reproduced with permission from Pedersen et al. [45] © WILEY-VCH Verlag GmbH & Co. KGaA 2008.

SHG profile in **Figure 8(a)** shows a strong wavelength-dependent behavior. At a pumping wavelength below two times of the band gap, d_{eff} gradually increases and reaches a maximum close to 760 nm and then varies slowly at higher pumping wavelength.

4.2. Dependence on aspect ratio

It is observed that the second-order nonlinear optical coefficients are strongly modified by dimensions of the NWs and aspect ratio. Chan et al. [13] and later Das et al. [14] demonstrated that changing of the aspect ratio of the ZnO nanorods could lead to a stronger SHG signal. ZnO NWs with different dimensions were grown by chemical method for different growth times, having diameter 10 to 62 nm and length 57 to 667 nm, respectively. Influence of aspect ratio on d_{31} and d_{33} is shown in **Figure 9** with aspect ratios ranging from 5.7 to 10.8. Interestingly, both the nonlinear second-order coefficients, d_{31} and d_{33}, were found to increase with increasing aspect ratio. The observed enhancement of d_{ij} is closely related to local field effects associated to the elongated nanorod structure. As we know, only d_{31} is excited when pumping beam is polarized along the rod's diameter. On the other hand, d_{33} being excited along the rod's longitudinal axis, the local field effect enhancement is predominantly connected to the rod's length. Similar effect on enhancement of d_{eff} was presented by Das et al. [14] for ZnO NWs with different length and diameters. Three different samples were grown with diameters 56, 59, and 95 nm and lengths 1300, 870, and 1020 nm, respectively. Calculated d_{eff} values are found to be 15.0, 2.0, and 3.2 pm/V, which is in correlation with the nanorod's length only. Later, a relationship between nanorod's diameter/length (aspect ratio) and corresponding $\chi^{(2)}$ values was established based on Lorentz local field, both theoretically and experimentally by Zhou et al. [37]. Theoretically, Lorentz local field-induced spectral red shift and the consequent dielectric constant modification were used to elucidate the size effect. The maximal value of $\chi_{31}^{(2)}$ of NW is the same as its bulk nonlinear susceptibility, while the maximum of $\chi_{33}^{(2)}$ of NW is significantly larger than its bulk counterpart. Therefore, the local field enhancement effect is more dominant along the longitudinal axis of NWs.

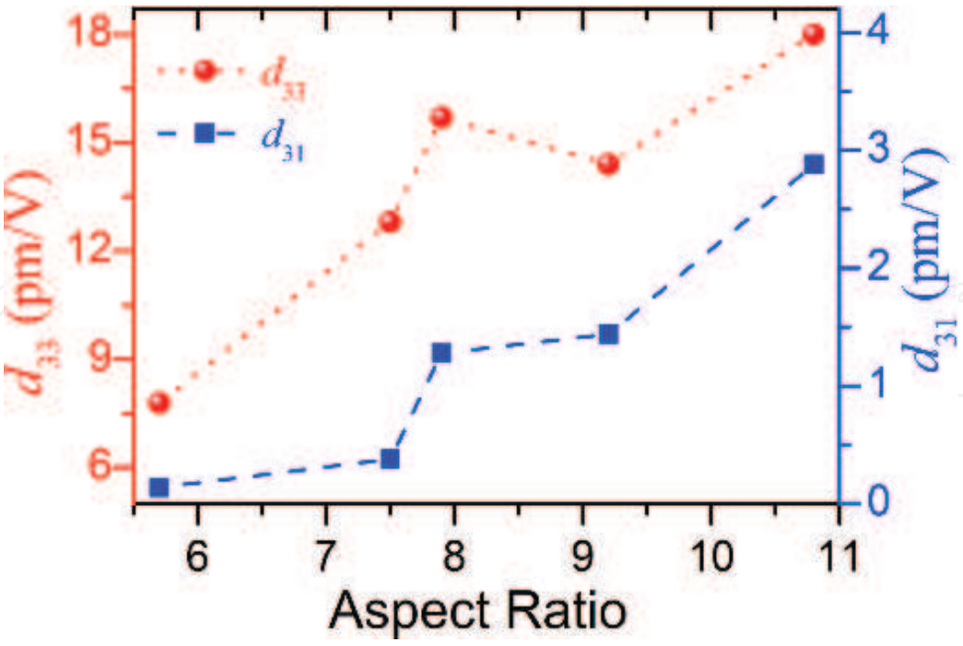

Figure 9. Dependences of d_{31} and d_{33} with the aspect ratio of ZnO nanowires.

4.3. The effect of doping

In order to improve the magnitude of the SHG in ZnO NWs, our group developed a technique to modify the crystal site symmetry of the ZnO crystal through rare earth element (Eu) doping [20]. We were able to improve the SHG about four times higher than the undoped ZnO NWs. That was the first ever report that used crystal symmetry modification technique to improve SHG. In the first step, Eu-doped ZnO (Eu:ZnO) NWs were grown vertically on the ZnO-seeded quartz substrate by a modified low temperature aqueous chemical method, using europium nitrate doping precursor. To facilitate the incorporation of larger Eu ions than the Zn ions into the ZnO lattice, a modification was done in the standard aqueous chemical method [49–52]. Eu doping was performed in a controlled way and a set of samples were prepared for different concentrations of Eu ranging from 0.5 to 5.0 at.%. Incorporation of Eu inside the ZnO lattice causes modification in the crystal site symmetry by disturbing the internal lattice arrangement. Extensive structural analysis using XRD data and high-resolution lattice images reveals expansion of lattice spacing and existence of several lattice distortions, as shown in the inset in **Figure 10**. Due to the larger ionic radius of Eu ions and the charge imbalance, incorporation of Eu completely disturbed the inside lattice arrangement. It is expected that the existence of a "self-purification process" [53] may further disturb the lattice arrangement. As a result, the formation of several lattice distortions in the Eu:ZnO NWs and hence degradation of structural quality and modification of site symmetry around the doped ions are expected.

The SHG intensity is found to increase after Eu doping. A nonmonotonic enhancement in the SHG is observed with increase in europium concentration. Maximum SHG was obtained from the 1 at.% Eu:ZnO NWs with an enhancement factor of 4.5. The effective second-order

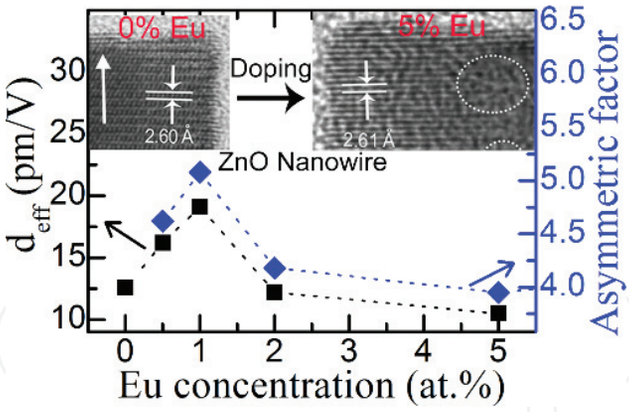

Figure 10. Plot of the d_{eff} and asymmetric factor (calculated from the PL intensity ratio) as a function of the Eu doping concentration for the Eu-doped ZnO nanowires. Inset shows high-resolution lattice image of the above undoped and 5 at.% Eu-doped ZnO NWs with growth orientation along <0001>. Formation of several lattice distortions in the Eu-doped ZnO nanowires is marked by dotted circles. Reproduced with permission from Dhara et al. [20] © IOP Publishing Ltd 2014.

nonlinear coefficient (d_{eff}) estimated from modified Maker fringes method is shown in **Figure 10** as a function of europium doping level. The highest d_{eff} (19.09 ± 0.11 pm/V) is obtained for the 1 at.% doped Eu:ZnO NWs, which is comparable to the value obtained by previous efforts to enhance the second-order susceptibility of ZnO thinfilms. Previous attempts to improve the second-order nonlinearity by changing the crystallographic orientation led to highest susceptibility ~30 pm/V [21] and decorating the surface with metal nanoparticles followed by bicolor coherent treatment led to the highest obtained susceptibility ~22.5 pm/V [54]. In comparison, our technique uses a simple process, whereas previous efforts were quite complicated from a technological point of view. Observed nonmonotonic enhancement was explained on the basis of Eu doping-induced symmetry deviation. The deviation in the crystal site symmetry (defined as the asymmetric factor) was estimated by employing photoluminescence (PL) spectroscopy and further supported by the microstructural characterizations. A strong correlation (linear dependence) is found between d_{eff} values and the magnitude of the asymmetric factor, which reveals that deviation in the local site symmetry around the Eu^{3+} ions in the Eu:ZnO crystal is the origin of the observed large second-order nonlinearity. Therefore, Eu doping on the ZnO NWs significantly influences the centrosymmetricity of the ZnO crystal, which results in an enhancement of the d_{eff} and hence SHG. This study opens up an avenue to improve the SHG of ZnO nanostructures through modification of local symmetry by incorporation of rare earth ions.

The effect of cobalt or thulium doping in ZnO NWs on the SHG characteristic was studied by other research group [40, 55]. Liu et al. [40] performed an SHG study after doping ZnO nanorods with cobalt. SHG was used to investigate bulk and surface structure quality of ZnO nanorods by measuring net dipole contribution for a different level of Co doping. Co-doped ZnO nanorods, $Zn_{1-x}Co_xO$ [$0 \le x \le 0.40$, x is the weight (wt.) % of Co in the growth solution], were fabricated by hydrothermal synthesis on seeded glass substrate. The SHG experiment was performed by varying incident angles in transmission mode (P-in/P-out configuration) with a femtosecond laser (1044 nm) light source. Ratios of d_{33} of Co-doped ZnO nanorods to

the undoped ones are 2.34, 1.06, and 0.59 for Co concentration of 1, 15, and 35 wt.%, respectively. Similar analysis found d_{31} to be 1.17, 0.83, and 1.48 for Co concentration of 1, 15, and 35 wt.%, respectively. Dilute Co concentration (1 wt.%) leads to larger d_{33} coefficient with maximum enhancement that leads to enhancement in the bulk crystal quality of ZnO nanorods.

4.4. External strain dependence

As we know, second harmonic generation depends on the nonzero second-order susceptibility tensor, which indeed depends on the crystal symmetry of that material. Now the question arises, can we modify the SHG in ZnO by applying external strain? To verify this, our group investigated external strain (tensile and compressive) dependent SHG in ZnO NWs after bending the NWs by applying external force [56]. In the first step, ZnO NWs were transferred from substrate and dispersed into a PMMA solution. The solution mixture was spin coated on a thin steel substrate (thickness 0.5 mm) to prepare a thin layer (~200 nm) of PMMA with horizontally aligned ZnO NWs within it. The PMMA thinfilm was heated at ~60°C to remove residuals and get a continuous film. External force was applied at the center of the substrate (opposite side of the film) to bend it along the radius of curvature of the substrate. The bending of substrate led to bending of the attached ZnO NWs and it experienced a strain on the surface, as shown in the inset of **Figure 11**. The PMMA matrix was used to hold the ZnO NWs during bending of the substrate. Applied strain at the center of the substrate along the direction of the applied force was estimated according to the strain equation developed earlier [57, 58].

We measured RSHG at an angle of incidence of 45° using a *p* polarized fundamental femtosecond pulse light tightly focused at the center of the substrate. The RSHG signal in both the stretched side and compressed side of the ZnO NWs were measured with increasing strain and then with decreasing strain (**Figure 11**). Stretched side of the NWs experienced tensile strain whereas compressed side experienced compressive strain. With increasing tensile strain, the SHG intensity first increases up to a certain amount of tensile strain and then decreases to the initial value with further strain. The magnitude of SHG trace during release of tensile strain showed reproducible strain-dependent characteristic. Maximum enhancement was obtained

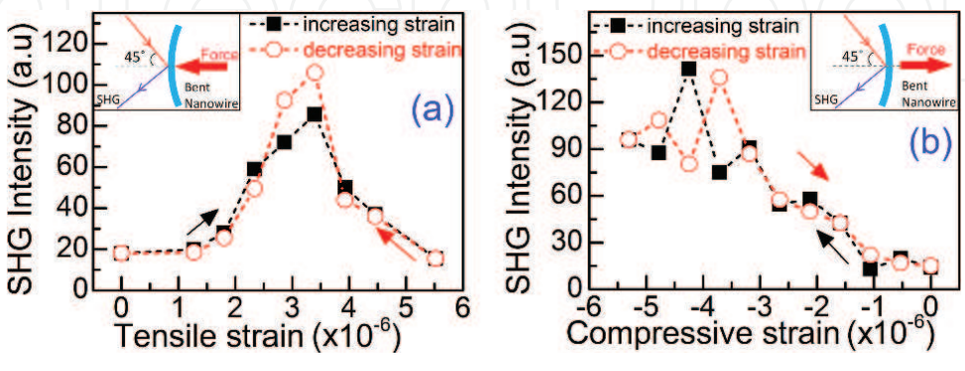

Figure 11. External strain-dependent RSHG intensity of bent ZnO NWs plotted as a function of (a) tensile strain and (b) compressive strain. SHG was measured by applying strain (black arrow, increasing strain) and then releasing strain (red arrow, decreasing strain). Insets show the measurement geometry of the bent ZnO NWs with external applied force (solid arrow).

about 400% at a tensile strain of 3.39×10^{-6}. On the other hand, SHG intensity gradually increases with increase in compressive strain. Reproducible SHG characteristic during release of compressive strain was also observed. At a compressive strain of 3.39×10^{-6}, obtained enhancement was about 430%. Therefore, SHG intensity in ZnO NWs could be enhanced and tuned through incorporation of external strain, either tensile or compressive.

5. Conclusion and future outlook

In this chapter, an up-to-date summary of important studies and results by several research groups worldwide on the SHG of ZnO NWs/nanorods is demonstrated. We present an extensive analysis and discussion on some key parameters that directly modify the efficiency of SHG in ZnO NWs. The key parameters considered for discussion are aspect ratio of NWs, doping, and external strain. Sample growth techniques, SHG measurement parameters, and extracted values of the nonlinear second-order coefficients from all the important studies are tabulated in **Table 1**. Most SHG studies are conducted on ZnO NWs with *c*-axis orientation (perpendicular to substrate) since their geometries allow to prepare *c*-axis–oriented vertically aligned structure, while only few studies deal with NWs with *c*-axis parallel to substrate. A significant advancement has been made in the improvement of nonlinearity of ZnO NWs, hence SHG intensity. Modified ZnO NWs now can compete with the existing standard nonlinear crystals. However, its needs further optimization and tailoring to get the maximum second-order nonlinearity. Fabrication of nonlinear optical devices using SHG characteristic of the ZnO NWs is certainly one of the future research directions.

Author details

Soumen Dhara[1]* and Stephen A. Lynch[2]

*Address all correspondence to: soumen5484@yahoo.co.in

1 Department of Condensed Matter Physics and Materials Sciences, S. N. Bose National Centre for Basic Sciences, Salt Lake, Kolkata, India

2 School of Physics and Astronomy, University of Cardiff, Cardiff, United Kingdom

References

[1] Kumar N, Dorfman A, Hahm J. Ultrasensitive DNA sequence detection using nanoscale ZnO sensor arrays. Nanotechnology. 2006;**17**:2875–2881

[2] Cui Y, Wei Q, Park H, Lieber CM. Nanowire nanosensors for highly sensitive and selective detection of biological and chemical species. Science. 2001;**293**:1289–1292

[3] Bano N, Zaman S, Zainelabdin A, Hussain S, Hussain I, Nur O, et al. ZnO-organic hybrid white light emitting diodes grown on flexible plastic using low temperature aqueous chemical method. Journal of Applied Physics. 2010;**108**:043103

[4] Fu X-W, Liao Z-M, Zhou Y-B, Wu H-C, Bie Y-Q, Xu J, et al. Graphene/ZnO nanowire/graphene vertical structure based fast-response ultraviolet photodetector. Applied Physics Letters. 2012;**100**:223114

[5] Johnson JC, Yan H, Schaller RD, Haber LH, Saykally RJ, Yang P. Single nanowire laser. The Journal of Physical Chemistry B. 2001;**105**:11387–11390

[6] Fiebig M, Pavlov VV, Pisarev RV. Second-harmonic generation as a tool for studying electronic and magnetic structures of crystals: Review. Journal of the Optical Society of America B. 2005;**22**:96−118

[7] Eisenthal KB. Second harmonic spectroscopy of aqueous nano- and microparticle interfaces. Chemical Review. 2006;**106**:1462–1477

[8] Campagnola P. Second harmonic generation imaging microscopy: Applications to diseases diagnostics. Analytical Chemistry. 2011;**83**:3224–3231

[9] Chen X, Nadiarynkh O, Plotnikov S, Campagnola PJ. Second harmonic generation microscopy for quantitative analysis of collagen fibrillar structure. Nature Protocols. 2012;**7**:654–669

[10] Castet F, Rodriguez V, Pozzo J-L, Ducasse L, Plaquet A, Champagne B. Design and characterization of molecular nonlinear optical switches. Accounts of Chemical Research. 2013;**46**:2656–2665

[11] Cao H, Wu JY, Ong HC, Dai JY, Chang RPH. Second harmonic generation in laser ablated zinc oxide thin films. Applied Physics Letters. 1998;**73**:572

[12] Griebner U, Kaindl RA, Elsaesser T, Seeber W. Frequency doubling and autocorrelation studies of 20-fs pulses using polycrystalline zinc oxide thin films. Applied Physics B. 1998;**67**:757–760

[13] Chan SW, Barille R, Nunzi JM, Tam KH, Leung YH, Chan WK, et al. Second harmonic generation in zinc oxide nanorods. Applied Physics B. 2006;**84**:351–355

[14] Das SK, Bock M, O'Neill C, Grunwald R, Lee KM, Lee HW, et al. Efficient second harmonic generation in ZnO nanorod arrays with broadband ultrashort pulses. Applied Physics Letters. 2008;**93**:181112

[15] Lo K-Y, Lo S-C, Yu C-F, Tite T, Huang J-Y, Huang Y-J, et al. Optical second harmonic generation from the twin boundary of ZnO thin films grown on silicon. Applied Physics Letters. 2008;**92**:091909

[16] Huang Y-J, Lo K-Y, Liu C-W, Liu C-C, Chu S-Y. Characterization of the quality of ZnO thin films using reflective second harmonic generation. Applied Physics Letters. 2009;**95**:091904

[17] Shi SL, Xu SJ, Xu Z-X, Roy VAL, Che C-M. Broadband second harmonic generation from ZnO nano-tetrapod. Chemical Physics Letters. 2011;**506**:226–229.

[18] Zheng CC, Xu SJ, Ning JQ, Zhang SF, Wang JY, Che CM, et al. Inner surface enhanced femtosecond second harmonic generation in thin ZnO crystal tubes. Journal of Applied Physics. 2011;**109**:013528

[19] Lu X, Zhou H, Salamo GJ, Tian ZR, Xiao M. Generation of exciton-polaritons in ZnO microcrystallines using second-harmonic generation. New Journal of Physics. 2012;**14**:073017

[20] Dhara S, Imakita K, Mizuhata M, Fuji M. Europium doping induced symmetry deviation and its impact on the second harmonic generation of doped ZnO nanowires. Nanotechnology. 2014;**25**:225202.

[21] Kityk IV, Ebothe J, Elchichou A, Addou M, Bougrine A, Sahraoui B. Linear electro-optics effect in ZnO–F film–glass interface. Physica Status Solidi B. 2002;**234**:553–562.

[22] Hyun JK, Kang T, Baek H, Oh H, Kim D-S, Yi G-C. Enhanced second harmonic generation by coupling to exciton ensembles in Ag-coated ZnO nanorods. ACS Photonics. 2015;**2**:1314−1319.

[23] Yang M, Shen S, Wang X, Yu B, Huang S, Xu D, et al. Plasmon-enhanced second-harmonic generation from hybrid ZnO-covered silver-bowl array. Journal of Physics: Condensed Matter. 2016;**28**:214003.

[24] Ren M-L, Agarwal R, Liu W, Agarwal R. Crystallographic characterization of II−VI semiconducting nanostructures via optical second harmonic generation. Nano Letters. 2015;**15**:7341−7346.

[25] Han X, Wang K, Long H, Hu H, Chen J, Wang B, et al. Highly sensitive detection of the lattice distortion in single bent ZnO nanowires by second-harmonic generation microscopy. ACS Photonics. 2016;**3**:1308−1314.

[26] Franken PA, Hill AE, Peters CW, Weinreich G. Generation of optical harmonics. Physical Review Letters. 1961;**7**:118.

[27] Rumpel A, Manschwetus B, Lilienkamp G, Schmidt H, Daum W. Polarity of space charge fields in second-harmonic generation spectra of Si(100)/SiO_2 interfaces. Physical Review B. 2006;**74**:081303.

[28] Jun B, White YV, Schrimpf RD, Fleetwood DM, Brunier F, Bresson N, et al. Characterization of multiple Si/SiO_2 interfaces in silicon-on-insulator materials via second-harmonic generation. Applied Physics Letters. 2004;**85**:3095–3097.

[29] Maker PD, Terhune RW, Nisenhoff M, Savage CM. Effects of dispersion and focusing on the production of optical harmonics. Physical Review Letters. 1962;**8**:21–22.

[30] Herman WN, Hayden LM. Maker fringes revisited: Second-harmonic generation from birefringent or absorbing materials. Journal of the Optical Society of America B. 1995;**12**:416–427.

[31] Attaccalite C, Nguer A, Cannuccia E, Gruning M. Strong second harmonic generation in SiC, ZnO, GaN two-dimensional hexagonal crystals from first-principles many-body calculations. Physical Chemistry Chemical Physics. 2015;**17**:9533–9540.

[32] Dhara S, Imakita K, Mizuhata M, Fujii M. Eu-doping induced improvement on the second harmonic generation of ZnO Nanowires. In: Jagadish C, editor. Materials Research Society Symposium Proceedings; 2014. pp. 95–100; DOI: 10.1557/opl.2014.367

[33] Wang G, Wong GL, Ketterson JB. Redetermination of second-order susceptibility of zinc oxide single crystals. Applied Optics. 2001;**40**:5436

[34] Johnson JC, Yan H, Schaller RD, Petersen PB, Yang P, Saykally RJ. Near-field imaging of nonlinear optical mixing in single ZnO nanowires. Nano Letters. 2002;**2**:279–283

[35] Geren K, Liu SW, Zhou HJ, Zhang Y, Tian R, Xiao M. Second-order susceptibilities of ZnO nanorods from forward second-harmonic scattering. Journal of Applied Physics. 2009;**105**:063531.

[36] Das M, Rana S, Sen P. Second harmonic generation in ZnO nanorods. The Journal of Nonlinear Optical Physics & Materials. 2010;**19**:445–458.

[37] Zhou G-Y, Hsu K-J, Su T-Y, Huang N-H, Chen Y-F, Chu S-W. Effect of Lorentz local field for optical second order nonlinear susceptibility in ZnO nanorod. Journal of Applied Physics. 2012;**111**:103112.

[38] Liu W, Wang K, Long H, Chu S, Wang B, Lu P. Near-resonant second-order nonlinear susceptibility in c-axis oriented ZnO nanorods. Applied Physics Letters. 2014;**105**:071906.

[39] Liu C-W, Chang S-J, Huang C-HHR-J, Lin Y-S, Su M-C, Wang P-H, et al. Probing surface structure quality of ZnO nanorods by second harmonic generation. IEEE Photonics Technology Letters. 2014;**26**:789–792.

[40] Liu C-W, Chang S-J, Brahma S, Hsiao C-H, Chang FM, Wang PH, et al. Enhancement in the structure quality of ZnO nanorods by diluted Co dopants: Analyses via optical second harmonic generation. Journal of Applied Physics. 2015;**117**:084315.

[41] Panda R, Bhattacharya S, Samal R, Singh A, Sahoo PK, Datta PK, et al. Second harmonic generation of femtosecond pulses using ZnO nanorods grown by chemical bath deposition with drop casted seed layer. Journal of Nonlinear Optical Physics & Materials. 2016;**25**:1650029.

[42] Kulyk B, Essaidi Z, Kapustianyk V, Turko B, Rudyk V, Partyka M, et al. Second and third order nonlinear optical properties of nanostructured ZnO thin films deposited on α-BBO and $LiNbO_3$. Optics Communications. 2008;**281**:6107–6111.

[43] Narayanan V, Thareja RK. Harmonic generation in ZnO nanocrystalline laser deposited thin films. Optics Communications. 2006;**260**:170–174.

[44] Liu SW, Zhou HJ, Ricca A, Tian R, Xiao M. Far-field second-harmonic fingerprint of twinning in single ZnO rods. Physical Review B. 2008;**77**:113311.

[45] Pedersen K, Fisker C, Pedersen TG. Second-harmonic generation from ZnO nanowires. Physica Status Solidi C. 2008;**5**:2671–2674.

[46] Prasanth R, Vugt LKV, Vanmaekelbergh DAM, Gerritsen HC. Resonance enhancement of optical second harmonic generation in a ZnO nanowire. Applied Physics Letters. 2006;**88**:181501.

[47] Zhang CF, Dong ZW, You GJ, Zhu RY, Qian SX, Deng H, et al. Femtosecond pulse excited two-photon photoluminescence and second harmonic generation in ZnO nanowires. Applied Physics Letters. 2006;**89**:042117.

[48] Das SK, Biswas M, Byrne D, Bock M, McGlynn E, Breusing M, et al. Multiphoton-absorption induced ultraviolet luminescence of ZnO nanorods using low-energy femtosecond pulses. Journal of Applied Physics. 2010;**108**:043107.

[49] Greene LE, Law M, Goldberger J, Kim F, Johnson JC, Zhang Y, et al. Low-temperature wafer-scale production of ZnO nanowire arrays. Angewandte Chemie International Edition. 2003;**42**:3031–3034.

[50] Xu S, Wang ZL. One-dimensional ZnO nanostructures: Solution growth and functional properties. Nano Research. 2011;**4**:1013–1098.

[51] Tak Y, Yong K. Controlled growth of well-aligned ZnO nanorod array using a novel solution method. The Journal of Physical Chemistry B. 2005;**109**:19263–19269.

[52] Dhara S, Giri PK. Ti nanoparticles decorated chemically grown ZnO nanowires: Photocurrent and photoluminescence properties. Journal of Experimental Nanoscience. 2013;**8**: 332–340.

[53] Gustavo MD, James RC. Self-purification in semiconductor nanocrystals. Physical Review Letters. 2006;**96**:226802.

[54] Ozga K, Kawaharamura T, Umar AA, Oyama M, Nouneh K, Slezak A, et al. Second order optical effects in Au nanoparticle-deposited ZnO nanocrystallite films. Nanotechnology. 2008;**19**:185709.

[55] Aloufy A, Ebothé J, Dumelié N, Chaki I, Abd-Lefdil M, AlZayed NS, et al. Optically stimulated optical effects in the ZnO:Tm nanorods. Physica E. 2015;**73**:96–99.

[56] Dhara S, Imakita K, Mizuhata M, Fuji M. External strain dependent anomalous second harmonic generation in ZnO nanowires film. (unpublish work).

[57] Liarokapis E, Papadimitriou D, Rumberg J, Richter W. Raman and RAS measurements of uniaxially strained thin semiconductor layer. Physica Status Solidi B. 1999;**211**:309–316.

[58] Zhao J-H, Chen Q-D, Chen Z-G, Jia G, Su W, Jiang Y, et al. Enhancement of second-harmonic generation from silicon stripes under external cylindrical strain. Optics Letters. 2009;**34**:3340–3342.